# Interaction between an inclined gravity current and a pycnocline in a two-layer stratification

**Yukinobu Tanimoto**[1,†]**, Nicholas T. Ouellette**[1] **and Jeffrey R. Koseff**[1]

[1]The Bob and Norma Street Environmental Fluid Mechanics Laboratory, Department of Civil and Environmental Engineering, Stanford University, Stanford, CA 94305-4020, USA

A series of laboratory experiments were conducted to investigate the characteristics of a dense gravity current flowing down an inclined slope into a quiescent two-layer stratification. The presence of the pycnocline causes the gravity current to split and intrude into the ambient at two distinct levels of neutral buoyancy, as opposed to the classical description of gravity currents in stratified media as being either a pure underflow or interflow. The splitting behaviour is observed to be dependent on the Richardson number ($Ri_\rho$) of the gravity current, formulated as the ratio of the excess density and the ambient stratification. For low $Ri_\rho$, underflow is more dominant, while at higher $Ri_\rho$ interflow is more dominant. As $Ri_\rho$ increases, however, we find that the splitting behaviour eventually becomes independent of $Ri_\rho$. Additionally, we have also identified two different types of waves that form on the pycnocline in response to the intrusion of the gravity current. An underflow-dominated regime causes a pycnocline displacement where the speed of the wave crest is locked to the gravity current, whereas an interflow-dominated regime launches an internal wave that moves much faster than the gravity current head or interfacial intrusion.

**Key words:** gravity currents, internal waves

---

## 1. Introduction

Gravity currents are nearly horizontal flows driven by lateral density gradients (Simpson 1982, 1997). They play a key role in the transport of scalars in a range of environmental settings, including dense inflows into lakes (Fischer & Smith 1983; Hogg *et al.* 2013; Cortés *et al.* 2014*a*), snow avalanches (Sovilla, McElwaine & Köhler 2018), katabatic winds down mountain faces and valleys (Samothrakis & Cotel 2006*b*), turbidity currents and mudslides (MacIntyre *et al.* 1999; Marti & Imberger 2008), volcanic lava gravity currents (Huppert & Dade 1998) and effluent discharges (Rueda, Fleenor & de Vicente 2007; Baines 2008; Meiburg & Kneller 2010; Hodges, Furnans & Kulis 2011). When an inclined gravity current descends down a slope, it entrains ambient fluid and is gradually diluted as it flows (Ellison & Turner 1959; Hebbert *et al.* 1979; Dallimore, Imberger & Ishikawa 2002; Fernandez & Imberger 2006; Cenedese & Adduce 2010). Gravity currents propagating in homogeneous environments have been extensively studied in the laboratory, leading

† Email address for correspondence: ytanimoto@stanford.edu

to well-developed characterizations of the entrainment and frontal structure (Benjamin 1968; Britter & Simpson 1978; Simpson & Britter 1979; Britter & Linden 1980; Hallworth *et al.* 1996; Odier, Chen & Ecke 2012, 2014), mixing and entrainment at the interface (Krug *et al.* 2015) and propagation along spatially varying bathymetry (Negretti, Flòr & Hopfinger 2017).

When the receiving ambient is stratified, the fate and transport of the gravity current become more complex than in a homogeneous environment (Monaghan 2007). In the stratified case, the gravity current will insert itself into the ambient at a depth where its fluid is neutrally buoyant (Fischer *et al.* 1979; Turner 1986; Chapra 1997; Baines 2001). Researchers have examined the structure and propagation of purely intrusive gravity currents in stratified ambients using both theoretical analyses and laboratory experiments (Holyer & Huppert 1980; Britter & Simpson 1981; Lowe, Linden & Rottman 2002; Flynn & Sutherland 2004; Sutherland, Kyba & Flynn 2004; Cheong, Kuenen & Linden 2006), as well as gravity currents propagating at the base of a stratified ambient (Maxworthy *et al.* 2002; Ungarish & Huppert 2002). In two-layer stratifications, such as below the wind mixed layer in the ocean, a gravity current will either intrude at the pycnocline, if it is lighter than the lower layer, or split into an intrusion at the pycnocline and a gravity current descending beneath the lower ambient layer, if it contains fluid denser than the lower layer (Monaghan *et al.* 1999; Samothrakis & Cotel 2006*b*; Monaghan 2007; Wells & Wettlaufer 2007; Mott & Woods 2009; Cortés *et al.* 2014*a*; Cortés, Rueda & Wells 2014*b*).

Monaghan *et al.* (1999) examined a dense gravity current descending into a two-layer stratified system and observed solitary internal wave generation and the splitting of the gravity current, but the splitting was not quantified or predictable. In similar experiments, Samothrakis & Cotel (2006*a*,*b*) investigated the changes in vorticity and velocity for a gravity current before and after the pycnocline, for both finite-volume and continuous releases. They found that both quantities increased after impinging on the pycnocline for supercritical gravity currents and decreased for subcritical gravity currents. Cortés *et al.* (2014*b*) developed a predictive framework for the splitting of a gravity current using both the density and velocity profile of the gravity current before the impingement on the pycnocline, and found good agreement with numerical experiments in Cortés *et al.* (2015). However, in many environmental flows the exact density and velocity profiles are not known.

Motion in the ambient fluid has also been shown to exert a significant influence on the behaviour of the gravity current (Ellison & Turner 1959; Fischer & Smith 1983). For example, when there is a counter-flow, as occurs in estuarine salt wedges (Simpson 1997), the gravity current can be arrested or reversed and its thickness can be modified (Ellison & Turner 1959; Britter & Simpson 1978; Hallworth, Hogg & Huppert 1998). In addition, the collision of two gravity currents has been shown to generate reflected bores (Shin 2001). Finally, recent experiments on gravity currents propagating beneath free-surface waves showed that the gravity current motion was dominated by the gravity current density, with Stokes drift caused by the surface waves being only a second-order effect (Robinson, Eames & Simons 2013). Little research has been done on gravity currents propagating into turbulent environments. Linden & Simpson (1986) examined gravity currents in fluids with background turbulence generated by rising bubbles. They found that in the presence of strong background turbulence the head of the gravity current would not form and the advance of the gravity current was best modelled as a turbulent diffusion process rather than advection driven by density gradients. Gravity currents have also been shown to drive ambient motion by radiating internal waves in stratified fluids (Monaghan *et al.* 1999;

Maxworthy *et al.* 2002; Ungarish & Huppert 2002; Flynn & Linden 2006; Maurer & Linden 2014).

In addition to naturally occurring gravity currents, there is now an increasing need to consider the fate of anthropogenic gravity currents in the coastal environment, such as the discharge of brine effluents from seawater desalination facilities. These may be continuous or finite-volume releases, depending on the operating procedures of the facility (Roberts, Johnston & Knott 2010; Hodges *et al.* 2011; Lattemann & Amy 2013; Missimer & Maliva 2017). The extent to which brine plumes from these facilities have an impact on the coastal ocean remains very uncertain (Fernández-Torquemada *et al.* 2009; Jenkins *et al.* 2012), but they are likely to have significant ecological and economic consequences (Kvitek, Conlan & Iampietro 1998). Fundamental understanding of the mixing and transport of the plume in ambient receiving waters, which typically have strong internal wave action, is critical for predicting the concentrations of brine and chemical additives in the plume and the reduction in oxygen at the seabed beneath the brine (Hodges *et al.* 2011).

Although we are studying a quiescent ambient stratification, many stratified natural and engineered systems contain internal waves and seiches that are a significant source of kinetic energy that may affect the downslope transport of gravity currents (Fischer & Smith 1983; Turner 1986; Masunaga, Fringer & Yamazaki 2016). Fischer & Smith (1983) found in their field study that internal wave motions were responsible for transporting a portion of an initially negatively buoyant river inflow to the surface. Internal waves incident on slopes have been extensively studied in the laboratory (Troy & Koseff 2005*b*; Hult, Troy & Koseff 2011; Moore, Koseff & Hult 2016), numerical simulations (Venayagamoorthy & Fringer 2007; Arthur & Fringer 2014) and the field (Davis & Monismith 2011; Walter *et al.* 2012), and have been shown to greatly enhance vertical mixing when they break and shoal, resulting in a turbulent bolus propagating upslope. Recent experiments by Hogg *et al.* (2016, 2017) have demonstrated that a single oncoming internal wave can reduce the downslope mass flux of a gravity current by up to 40 %.

Although there is ultimately a need to understand the interaction between gravity currents and breaking internal waves on slopes, in this paper we focus on the zero-order question of the dynamics of gravity currents propagating into a stratified two-layered system with the goal of answering the following questions:

(i) How does the gravity current split, based on the initial conditions for the gravity current and the receiving ambient stratification?
(ii) How does the pycnocline in a two-layer stratification respond to different gravity currents?

In the following, we first provide details of our experimental facility and procedures, and an overview of the non-dimensional parameters that give the theoretical backdrop for our analyses in § 2. In § 3 we present the results from our experiments as well as a discussion of these results. Overall conclusions derived from our study are given in § 4.

## 2. Experimental methods

### 2.1. *Facility*

A series of experiments were performed in the Stratified Flow Facility in The Bob and Norma Street Environmental Fluid Mechanics Laboratory at Stanford University (see Troy & Koseff (2005*a*) and Moore *et al.* (2016) for more details). A schematic
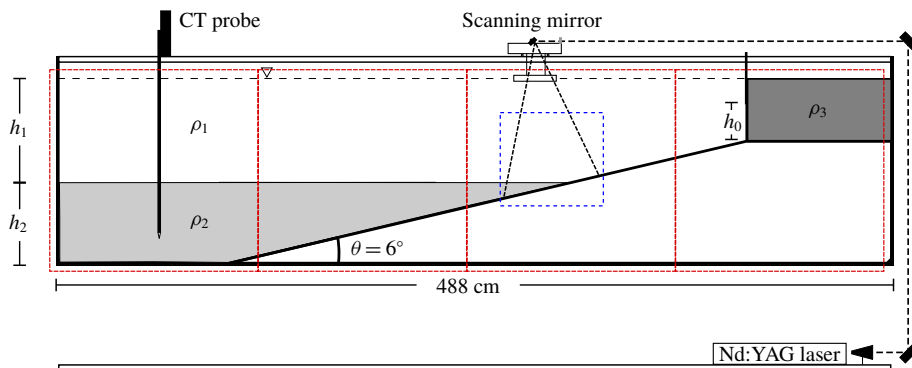
FIGURE 1. Schematic of the facility and measurement instrumentation. The blue box shows the region where PLIF was conducted, and the four red boxes show the fields of view of the cameras used to image the tracer dye.

of the experimental set-up is shown in figure 1. The facility consists of an enclosed rectangular tank 488 cm long, 60 cm tall and 30 cm wide fitted with an inclined slope of 6° caulked to the side of the tank. A lock that is 56 cm long and 10.6 cm deep at the top of the incline allows the gravity current fluid to be held in isolation from the rest of the tank before the experiment begins.

## 2.2. Procedure

A two-layer stratification was prepared following the methodology of Moore *et al.* (2016), using a floating diffuser to achieve an overall density difference of $\Delta\rho/\rho_0 = 2(\rho_2 - \rho_1)/(\rho_2 + \rho_1) = 1.2\%$ between the two ambient layers. The density of the upper layer was close to that of fresh water, although a small amount of NaCl was added to improve the performance of the conductivity probe (Precision Measurements Engineering, model 125) used to measure densities. The probe had a fast-response conductivity sensor ($-3$ dB at approximately 800 Hz) and fast thermistor (7 ms response time), allowing for accurate density measurements, and was traversed vertically at a speed of 10 cm s$^{-1}$. The upper-layer density was $\rho_1 \approx 1001$ kg m$^{-3}$, and the lower layer was set to a density of $\rho_2 \approx 1013$ kg m$^{-3}$. The gravity current fluid that was initially in the lock was set to a density $\rho_3$ ranging from 1017 to 1038 kg m$^{-3}$. All the fluid used in the experiments was allowed to equilibrate to the ambient laboratory temperature prior to the experiments to remove any temperature variability that could affect the density.

The upper- and lower-layer heights were kept constant at $h_1 = 21$ cm and $h_2 = 27.5$ cm, respectively, for all experiments, and the distance from the lock to the pycnocline was 100 cm as measured along the incline. Prior to initiating the experiments, the pycnocline region of intermediate density between the ambient layers was sharpened using a thin slotted pipe as described in Troy & Koseff (2005a). The interfacial thickness was calculated from a vertical density profile taken with the conductivity probe mounted on a vertical traverse as the thickness over which 99% of the density variations occurred, consistent with Fringer & Street (2003) and Troy & Koseff (2005a), and was held constant for all experiments at $1.4 \pm 0.2$ cm.

While stratifying the tank, the lock was closed off so that there was no mixing of the gravity current fluid with the tank fluid. At the start of the experiment, the lock

containing the gravity current was opened sharply to a prescribed gate opening height ($h_0$) allowing the gravity current to form on the slope. The partial gate opening is not an issue for the reproducibility of the experiments, and we found a very consistent relationship between the gravity current depth $h_c$ and the gate opening height $h_0$.

The volume of the gravity current was kept constant for all experiments at $16\,000$ cm$^3$, similar to that of the experiments of Samothrakis & Cotel (2006a) and other experiments summarized in table 3 of Samothrakis & Cotel (2006a). Vertical density profiles were taken at the downstream end of the tank where the bottom slope is horizontal both before and after the gravity current release. Profiling was continued for 2 h following the release of the gravity current to ensure that no horizontal gradients in the density field were present. A sampling port allowed density measurements to be taken at the bottom of the tank, as the probe was limited in its traversal to a few centimetres above the bottom. A hyperbolic tangent fit was used to extrapolate the bottom portion of the density profile to the measured density while enforcing the no-flux boundary condition on the density profile.

### 2.3. *Planar laser-induced fluorescence*

Planar laser-induced fluorescence (PLIF) was used to obtain the velocity, density and overall structure of the gravity current before it reached the pycnocline. The fluid was seeded with a laser-fluorescent dye (rhodamine 6G) with a Schmidt number similar to that of the salt used to stratify the fluid ($Sc = \nu/\kappa$ of 600–1200 and 700, respectively, where $\nu$ is the kinematic viscosity and $\kappa$ is the molecular diffusivity). The concentration of the laser-induced fluorescence dye was then directly related to the salinity field (Rehmann 1995).

A computer-controlled scanning mirror was used to generate a light sheet with a width of approximately 0.5 mm at its thinnest from a Nd:YAG laser beam, illuminating the dye in a two-dimensional plane along the centreline of the tank. The imaging domain is shown in figure 1, and was selected so that measurements of the gravity current could be taken before its interaction with the pycnocline. Images were acquired using a $2048 \times 2048$ pixel CCD camera (Redlake ES 4.0 with a SIGMA 30 mm F1.4 DC HSM lens), and the spatial resolution was 0.2 mm. The pixel intensity from the imaging was converted to dye concentration and then to density using the calibration methodology of Crimaldi & Koseff (2001) and Troy & Koseff (2005a). Images were acquired at a frame rate of 7.5 Hz. Using this approach, the density, frontal speed and height of the gravity current head could be measured. The frontal speed of the gravity current was determined in a manner similar to that of Simpson (1997), Venayagamoorthy & Fringer (2007) and Moore *et al.* (2016). Figure 2 shows a set of processed images acquired with PLIF showing the density gradients in the gravity current as well as the evolution of the frontal position of the gravity current.

### 2.4. *Flow visualization*

An array of four cameras (Basler acA2040-90um with TAMRON 16 mm F1.8 lenses, 0.8 mm resolution) was set up along the length of the tank (denoted by four red boxes in figure 1) to capture the progression of the gravity current, as well as other flow features, along the entirety of the tank, as opposed to the limited spatial extent of the PLIF camera. Dye (McCormick® Food Colouring) was added to the different ambient layers and the gravity current to distinguish the different fluids. Although the density of the fluid could not be extracted from these images, the gravity current speed
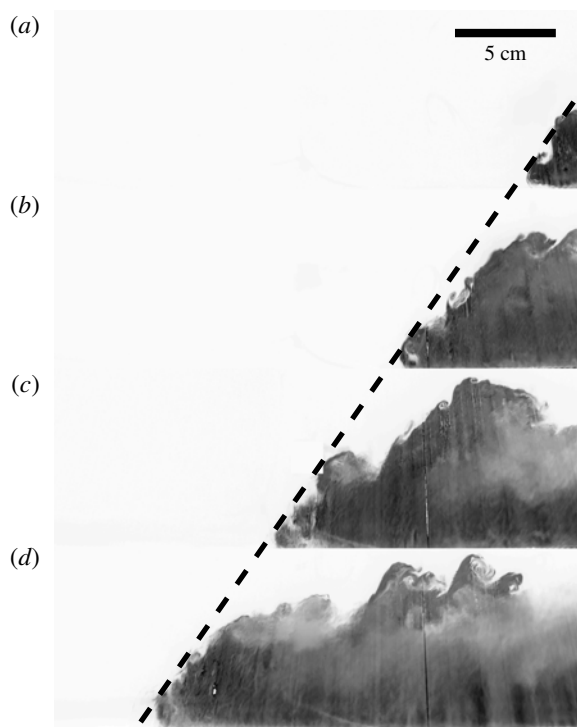
FIGURE 2. Image sequence of a gravity current propagating downslope. Images are shown at 0.53 s intervals. The frontal position of the gravity current moves at a constant speed, as indicated by the dashed straight line.

and any pycnocline movement could be quantified by processing them. The image acquisition was synchronized between all the cameras using an external function generator.

### 2.5. *Non-dimensional parameters*

The Richardson number, *Ri*, expressing the competition between buoyancy and shear, is typically used to characterize gravity current dynamics. However, various forms of the Richardson number appear in the literature and are appropriate for different situations. In the case of a gravity current released into a homogeneous ambient, Ellison & Turner (1959) and Britter & Linden (1980) found that the gravity current can be characterized by a Richardson number defined as

$$Ri = \frac{g'_{13} h \cos\theta}{U^2}, \tag{2.1}$$

where $g'_{13} = g(\rho_3 - \rho_1)/\rho_0$ is the reduced gravity calculated with the gravity current and ambient density and $h$ and $U$ are the height and mean velocity of the gravity current. The entrainment, or the rate at which the gravity current head grows, is a function of this Richardson number (Ellison & Turner 1959). This Richardson number can be also interpreted as a densimetric Froude number with the relation $Fr = Ri^{-2}$ to describe the criticality of the gravity current. The gravity currents in the present

study are all subcritical by this *Fr* criterion, whereas other studies such as Cortés *et al.* (2014*b*) examined both supercritical and subcritical gravity current regimes.

Wallace & Sheff (1987) proposed a different form of the Richardson number to predict and characterize the fate of a buoyant plume in a two-layer stratification. This formulation of *Ri* relates both the depth of the ambient layer into which the gravity current is released and the strength of the ambient stratification to the buoyancy flux of the gravity current, and is given by

$$Ri_\rho = \frac{g'_{12}h_1}{B^{2/3}}, \tag{2.2}$$

where $g'_{12} = g(\rho_2 - \rho_1)/\rho_0$ is the reduced gravity over the ambient stratification and $B = g'_{13}Q/b$ is the buoyancy flux per unit width, where $b$ is the width. For a negatively buoyant gravity current, shallow-water theory and dam-break theory predict the depth of the fluid leaving the lock gate as $h_c = 4/9h_0$ and the average velocity as $U_c = 2/3(g'_{13}h_0)^{1/2}$ (Acheson 1990), giving the buoyancy flux per width as $B = g'_{13}h_cU_c = 8/27(g'_{13}h_0)^{3/2}$. Britter & Linden (1980) found that the frontal speed of the gravity current is $U_f/B^{1/3} = 1.5 \pm 0.2$ independent of the slope for inclines in the range $5° \leqslant \theta \leqslant 90°$. Monaghan *et al.* (1999) found that $U_f/B^{1/3} = 1.0 \pm 0.1$ for slopes between 20° and 90°, whereas Samothrakis & Cotel (2006*b*) found that $U_f/B^{1/3} = 1.6 \pm 0.3$ for a slope of 6°. In our experiments, we find that $U_f/B^{1/3} = 0.93 \pm 0.1$, more consistent with the results of Monaghan *et al.* (1999). Our calculations of $U_f/B^{1/3}$ agree with values found in the literature suggesting that the buoyancy flux was calculated correctly, and that shallow-water theory holds. While the partial gate opening certainly affects the buoyancy flux, the effects are well captured by the theory, and as stated above are highly reproducible.

Using only the initial conditions of the experiment, we can also define a Grashof number describing the ratio of the buoyancy of the gravity current to viscous forces as

$$Gr = \frac{h_0\sqrt{g'_{13}h_0}}{\nu}. \tag{2.3}$$

A larger Grashof number indicates that the gravity current flow is dominated by buoyancy-driven inertia as opposed to viscous drag. In our experiments, *Gr* ranged from $3.2 \times 10^3$ to $1.9 \times 10^4$ so that the motion of the gravity current is indeed dominated by buoyancy. The Reynolds number

$$Re = \frac{hU_f}{\nu} \tag{2.4}$$

of the gravity current can also be calculated using the characteristic height and frontal speed of the gravity current, and ranged from $1.8 \times 10^3$ to $9.7 \times 10^3$ in our experiments.

## 3. Results

We focus on addressing two fundamental questions in this paper. First, as the gravity current passes through the density interface, does it split in the manner described by Cortés *et al.* (2014*b*) as a function of the Richardson number of the current? Second, what is the behaviour of the interface itself as the gravity current passes through it? In the following, we address each question in turn.

| Run number | $\rho_1$ (kg m$^{-3}$) | $\rho_2$ (kg m$^{-3}$) | $\rho_3$ (kg m$^{-3}$) | $h_0$ (cm) | $Ri_\rho$ | $Gr$ | $Re$ |
|---|---|---|---|---|---|---|---|
| 1 | 1000.81 | 1012.42 | 1037.36 | 10 | 1.5 | $1.9 \times 10^4$ | $9.7 \times 10^3$ |
| 2 | 1000.80 | 1012.58 | 1030.23 | 10 | 1.9 | $1.7 \times 10^4$ | $8.1 \times 10^3$ |
| 3 | 1000.81 | 1012.65 | 1022.53 | 10 | 2.6 | $1.5 \times 10^4$ | $6.3 \times 10^3$ |
| 4 | 1000.85 | 1012.49 | 1037.37 | 8 | 1.9 | $1.3 \times 10^4$ | $7.0 \times 10^3$ |
| 5 | 1000.90 | 1012.83 | 1030.28 | 8 | 2.4 | $1.2 \times 10^4$ | $5.9 \times 10^3$ |
| 6 | 1000.83 | 1012.67 | 1022.53 | 8 | 3.2 | $1.0 \times 10^4$ | $4.7 \times 10^3$ |
| 7 | 1000.77 | 1012.60 | 1037.90 | 6 | 2.5 | $8.8 \times 10^3$ | $4.9 \times 10^3$ |
| 8 | 1000.73 | 1012.60 | 1030.11 | 6 | 3.2 | $7.9 \times 10^3$ | $4.1 \times 10^3$ |
| 9 | 1000.65 | 1012.31 | 1022.23 | 6 | 4.3 | $6.9 \times 10^3$ | $3.3 \times 10^3$ |
| 10 | 1001.23 | 1013.07 | 1017.18 | 4 | 8.8 | $3.2 \times 10^3$ | $1.8 \times 10^3$ |
| 11 | 1001.06 | 1013.06 | 1023.09 | 4 | 6.4 | $3.7 \times 10^3$ | $2.2 \times 10^3$ |

TABLE 1. Parameters for the different experimental runs, where $\rho_1$ and $\rho_2$ are the densities of the upper and lower ambient layers, $\rho_3$ is the gravity current density and $h_0$ is the gate opening at the lock. Here $Ri_\rho$, $Gr$ and $Re$ are the Richardson number, Grashof number and Reynolds number of the current, respectively (see text for definitions).

### 3.1. *Behaviour of the gravity current*

We first describe our results in a qualitative way, and subsequently use a more quantitative analysis of the centre of mass of the water column to assess how the current distributes itself after passing through the interface. The experimental conditions are given in table 1. The first nine runs were each conducted twice, once using PLIF to capture the gravity current in the pre-pycnocline region of the incline and once with an array of cameras to track the subsequent movement of the pycnocline. We performed the runs separately because the tracer dye used in the latter experiments interferes with the laser-induced fluorescence in the PLIF experiments.

The propagation of the gravity current through the top ambient layer is similar to the homogeneous ambient case that has been extensively studied by, among others, Britter & Simpson (1978), Britter & Linden (1980) and Simpson (1997), where rapid entrainment due to Kelvin–Helmholtz instabilities at the interface between the gravity current and ambient fluid reduces the overall density in the gravity current as it propagates down the slope. PLIF images, as depicted in figure 2, show that the gravity current head consists of an array of ever-evolving vortices due to the constant baroclinic torque production of vorticity through the misalignment of the density and pressure gradient as well as the initial vorticity produced in the current boundary layer. The tail of the gravity current moves faster than the head of the current, contributing an additional source of growth of the head (Monaghan 2007). As with experiments of Monaghan *et al.* (1999), a return bore of the upper-layer fluid is generated in the gravity current lock, but the head of the gravity current reaches the pycnocline before the bore affects the flow. Furthermore, the draining flow observed in the last stages of the gravity current fluid leaving the lock does not influence the interaction of the gravity current head with the pycnocline, which occurs well before this.

Upon reaching the pycnocline, we typically observe that the gravity current splits into two parts: one that penetrates the pycnocline and continues to propagate downslope (figure 3c), and one that inserts itself into the ambient stratification at the pycnocline (figure 3a) (Samothrakis & Cotel 2006b; Monaghan 2007). Given the density structure of the water column, the part of the gravity current with a density exceeding that of the lower layer proceeds downslope as an underflow and the part
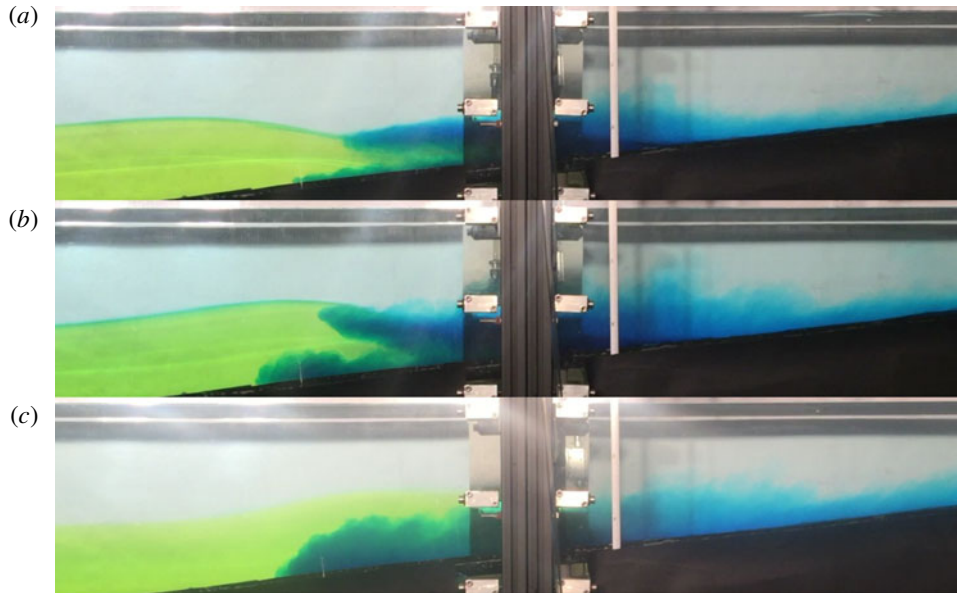
FIGURE 3. Splitting of the gravity current for different experimental conditions: (*a*) $Ri_\rho = 8.1$, showing a strong interflow; (*b*) $Ri_\rho = 3.7$, showing a splitting of the gravity current into an underflow and interflow; and (*c*) $Ri_\rho = 2.3$, where the gravity current is predominantly an underflow.

with a density less than that of the lower layer flows horizontally as an interflow. These flows are referred to as hyperpycnal and mesopycnal flows in sedimentology (Mulder & Alexander 2001). Through entrainment and mixing, an underflow can change the ambient stratification in the lower layer, whereas an interflow will result in a thickening of the pycnocline. In the following sections we quantify the amount of underflow and interflow for different experimental cases, and the subsequent pycnocline motions in response to an underflow or interflow.

### 3.1.1. *Splitting of the gravity current*

The vertical density profiles before and after the experiment can be used to quantify the extent of underflow or interflow. We consider multiple hypothetical outcomes, and compare those profiles to the actual experimentally measured profiles. Neglecting the case where the gravity current inserts into the ambient as a buoyant plume (in which the dynamics of the ambient two-layer stratification remains unaffected), three distinct limiting cases are possible and are discussed in detail below.

(*a*) Full interflow

In the case where the entrainment of the upper-layer fluid into the gravity current is significant, so that the density of the gravity current when it reaches the interface is less than that of the lower layer but slightly more than that of the upper layer, the entire volume of the gravity current will insert itself horizontally along the ambient pycnocline. In this full interflow scenario, the vertical extent of the ambient lower layer would not change, but the region of intermediate densities between the two layers will be thickened. This is shown schematically by the orange line with diamonds in figure 4.
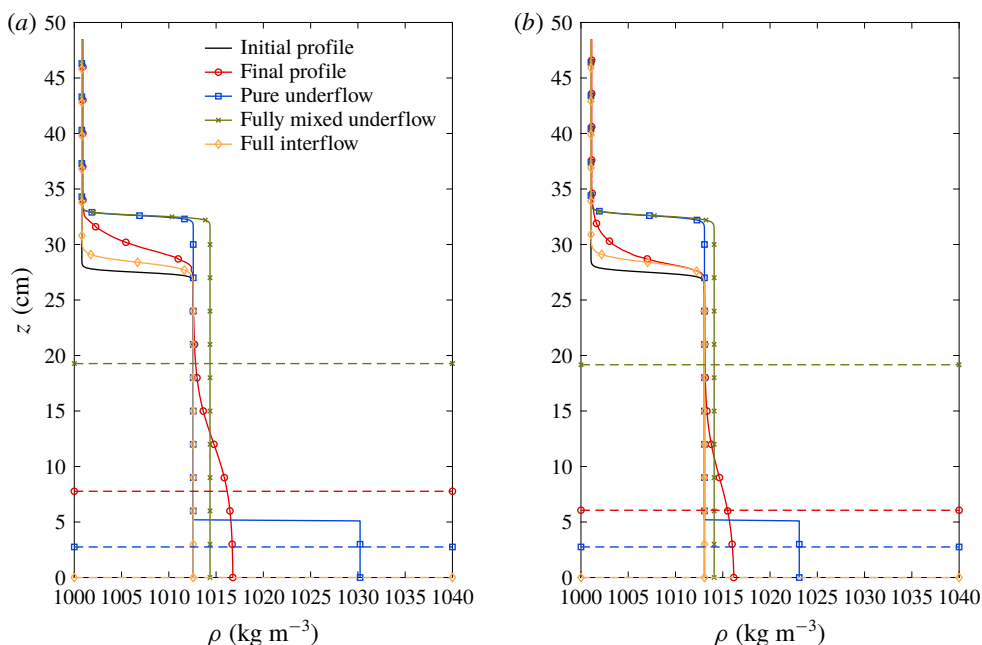
FIGURE 4. Comparison of measured and hypothetical vertical density profiles for (a) $Ri_\rho = 1.9$ and (b) $Ri_\rho = 6.4$. The horizontal lines indicate the centre of mass ($M_c$) for each density profile. The symbols have been added for clarification and do not reflect the sampling resolution.

(b) Fully mixed underflow

If the density of the gravity current remains close to its initial density as it reaches the pycnocline but then proceeds to mix completely with the lower ambient layer, the result is a fully mixed underflow. The lower-layer density is increased due to the additional density excess from the gravity current. The pycnocline thickness would be unaffected but it would be displaced upwards from the volumetric addition to the lower layer. This is shown schematically by the green line with asterisks in figure 4.

(c) Pure underflow

If the gravity current were immiscible with the ambient and therefore did not mix with either of the ambient layers, the current would insert itself with its original density at the bottom of the tank. This is the absolute lowest limit where a negatively buoyant gravity current could settle. In this case, the pycnocline thickness would remain unchanged but it would be displaced upwards from the underflow. This is shown schematically by the blue line with squares in figure 4.

(d) Experiments

Figure 4 shows the vertical density profiles for two separate inflow cases, $Ri_\rho = 1.9$ and $Ri_\rho = 6.4$, along with the hypothetical profiles described above. In the $Ri_\rho = 1.9$ case, the initial density of the gravity current is higher than that of the $Ri_\rho = 6.4$ case. Therefore, the gravity current signature in the immiscible underflow case shows a higher density in the $Ri_\rho = 1.9$ case than in the $Ri_\rho = 6.4$ case. Similarly, the lower-layer density in the fully mixed underflow case is higher for the $Ri_\rho = 1.9$ case than for the $Ri_\rho = 6.4$ case. In both measured final density profiles (red line with circles), the excess density from the gravity current underflow can be seen at

the bottom of the profiles. Below the pycnocline in the $Ri_\rho = 1.9$ case, the excess is present at around 20 cm, compared to around 15 cm in the $Ri_\rho = 6.4$ case. The density of the gravity current at the bottom has been reduced compared to its initial density due to entrainment while propagating through the ambient, consistent with experimental observations by Baines (2001) of gravity currents flowing into a continuous stratification.

The red lines with circles in figure 4 show the actual resultant density profiles for the two different flow cases superimposed on the theoretical profiles discussed above. The $Ri_\rho = 6.4$ case had a lower $g'_{13}$ and buoyancy flux, which suggests that, given that the velocity of the current is $U_f \sim B^{1/3}$, the time for it to pass through the upper-layer fluid was longer, and thus that there was more time for the gravity current to mix and entrain the upper-layer ambient fluid. The $Ri_\rho = 1.9$ case flowed through upper ambient faster owing to its higher velocity, leading to less time for mixing and entrainment. However, this effect was counterbalanced by the fact that the faster velocity also drove increased shear and mixing at the upper interface of the current. This reasoning may explain why the $Ri_\rho = 1.9$ case shows a more distributed profile above 28 cm suggesting increased mixing at higher (above the interface) vertical levels. For both final profiles, the pycnocline is displaced upwards due to the presence of the underflow. The $Ri_\rho = 6.4$ case shows a more asymmetric change in the density profile, with seemingly more fluid of a density closer to the upper layer present. This may be due to the interface intrusion that continues to entrain the upper layer as it propagates horizontally into the ambient.

Interestingly, we observe that some amount of interflow is always present, even in the lowest $Ri_\rho$ cases, consistent with previous experimental observations by Monaghan *et al.* (1999), Samothrakis & Cotel (2006*a*) and Cortés *et al.* (2014*b*). The experiments in Samothrakis & Cotel (2006*b*) and Cortés *et al.* (2014*b*) used a constant-buoyancy flux instead of a finite-volume gravity current release, and also exhibited an interflow even at low $Ri_\rho$. We offer the following explanation for this phenomenon, illustrated by a sequence of experimental images. In figure 5(*a*), a gravity current of $Ri_\rho = 1.3$ is descending downslope and has just reached the pycnocline. As the head of the gravity current penetrates the pycnocline (figure 5*b*), the pycnocline is displaced upwards, generating a pressure gradient that is positive for the gravity current head but adverse for the tail of the current. As a result, the head continues to propagate downward based on its initial downslope momentum (figure 5*c*) with the pressure gradient forcing the head downwards, but the tail is slowed down, causing the head to detach from the tail. The tail of the gravity current then continues to flow and mix into this region, which could explain the more distributed density profile seen in the pycnocline region for the $Ri_\rho = 1.9$ final profile in figure 4. The head continues downslope at a much higher velocity than the detached section, which then enters the ambient horizontally as an interflow (figure 5*d*) at a much slower velocity. By this mechanism, even gravity currents with very low $Ri_\rho$ will exhibit some detachment and create an interflow.

(*e*) Centre of mass

To quantify these effects, for each of the hypothetical density profiles and the measured final profile discussed above, we computed the centre of mass of the fluid with density greater than that of the original lower-layer density ($\rho_2$):

$$\rho(z) = \rho(z) - \rho_2. \tag{3.1}$$

By subtracting $\rho_2$ and computing the centre of mass, any fluid that is displaced upwards due to an underflow will not affect the calculation. The centre of mass, $M_c$,
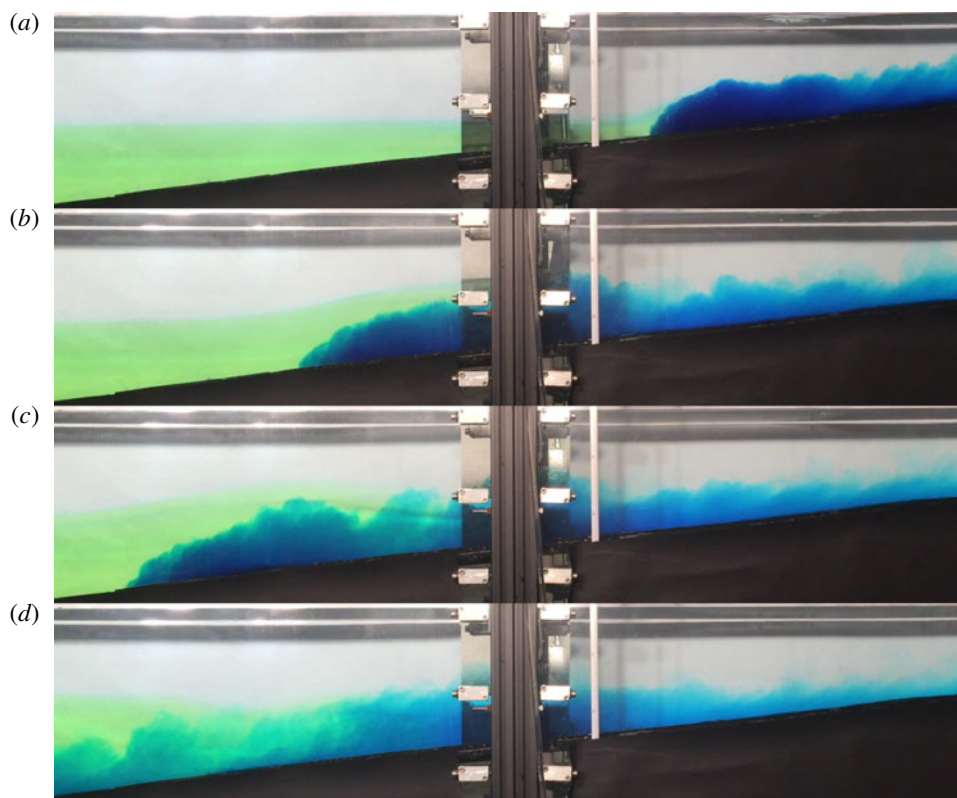
FIGURE 5. Progressive snapshots of a gravity current with $Ri_\rho = 1.3$ descending downslope. (*a*) The gravity current has just reached the pycnocline; (*b*) the head has passed through the pycnocline; and (*c*) the head has detached from the rest of the gravity current. (*d*) The intrusion at the interface propagates much more slowly than the head, which has exited to the left.

of this adjusted profile is then calculated as

$$M_c = \frac{\int_z \rho(z)A(z)z\,\mathrm{d}z}{\int_z \rho(z)A(z)\,\mathrm{d}z}, \tag{3.2}$$

where $A(z)$ is the vertical profile of the cross-sectional area. Computed in this way, the maximum (highest) centre of mass possible is for the fully mixed underflow case, where the density of the lower layer has been increased due to mixing of the gravity current. The unmixed underflow case gives the minimum (lowest) possible centre of mass, and these two cases provide bounds so that we can compute a normalized centre of mass $M_c^*$ as

$$M_c^* = \frac{M_{c,Final} - M_{c,PU}}{M_{c,FMU} - M_{c,PU}}. \tag{3.3}$$

In this equation $M_{c,PU}$ is the unmixed case, $M_{c,FMU}$ is a fully mixed underflow case and $M_{c,Final}$ is the actual measured centre of mass from each experiment. A gravity
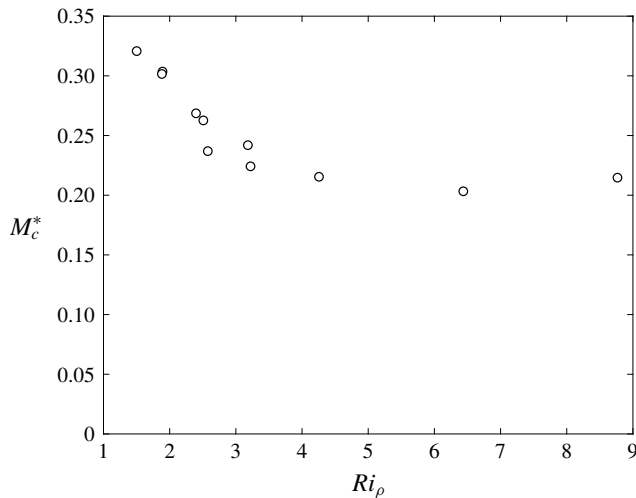
FIGURE 6. Normalized centre of mass of the gravity current in the lower layer as a function of the Richardson number. Errors propagated from the uncertainty in the measurements are smaller than the symbol size.

current that results in complete interflow would give a normalized centre of mass of $-0.1$, as the final centre of mass would be 0.

From figure 4, we see that the increased mixing and entrainment due to the higher shear in the lower $Ri_\rho$ cases leads to a higher centre of mass of the final profile compared to the higher $Ri_\rho$ cases (8 cm versus 6 cm). We can then compute the non-dimensional centres of mass for these cases as well as all the others shown in table 1. Figure 6 shows the non-dimensional centre of mass for the different experimental cases as a function of $Ri_\rho$. For reference, a fully mixed underflow would have a non-dimensional centre of mass of 1, and an unmixed underflow would have a non-dimensional centre of mass of 0. The maximum value from the experiments was 0.33 for the lowest $Ri_\rho$ case, well below the theoretical maximum of 1, which may be impossible to achieve as mixing will always occur between the gravity current and ambient fluid as long as the fluids are miscible.

The non-dimensional centre of mass is strongly dependent on the Richardson number for $Ri_\rho < 3.5$, with the ratio of underflow to interflow decreasing with increasing $Ri_\rho$. Even though there is less shear and subsequent mixing resulting in a less diluted gravity current as it enters the interface with increasing $Ri_\rho$, there is also a smaller buoyancy flux, making it less likely for a gravity current to be able to penetrate the pycnocline. For $Ri_\rho > 3.5$, there appears to be no strong dependence of the dimensionless centre of mass on $Ri_\rho$. For this range of Richardson numbers, a small amount of underflow is typically observed, but the majority of the gravity current becomes an interflow, as long as the initial density of the gravity current is above the lower-layer density (Monaghan *et al.* 1999). The constant value of $M_c^*$ strongly suggests that the downward buoyancy flux and the local shear and entrainment are balanced for this $Ri_\rho$ range, and that beyond a 'critical' or 'transitional' value, the splitting behaviour of negatively buoyant gravity currents will be independent of $Ri_\rho$. Our experiments suggest that this transitional $Ri_\rho$ is roughly 3.5.

### 3.2. *Pycnocline response to the gravity current*

The presence of the ambient stratification greatly affects the flow of the gravity current. As noted by Samothrakis & Cotel (2006*b*) and Monaghan (2007), waves are generated as the gravity current flows through the pycnocline. Monaghan *et al.* (1999) compared the measured amplitude and phase speeds and compared them to theoretical values derived from classic solitary wave theory (Long 1956) and found good agreement in experiments where the density difference between the gravity current and upper layer was approximately 10 %, and the wave amplitudes were sufficiently large so that they could be measured (excess of 1 cm). Samothrakis & Cotel (2006*a*) also found similar solitary waves generated in their experiments, but the focus of their study was more on the entrainment and internal structure of the gravity current. Here we present a classification of the response of the pycnocline to the gravity current as seen in our experiments.

#### 3.2.1. *Locked wave*

As the gravity current propagates downslope in the underflow-dominated cases, the pycnocline above the gravity current is displaced upwards. The crest of the deflection of the pycnocline is located slightly behind the head of the gravity current (figure 7*a–c*). The speed of the crest was measured using time-resolved imaging of the downslope location of the crest. In some of the experiments it is approximately equal to the frontal speed of the head of the gravity current, similar to the locked case observed in the supercritical regime in the experiments of Maxworthy *et al.* (2002). In other experiments the gravity current has intense vortical structures in its head and has evanescent Kelvin–Helmholtz instabilities that cause large billow-like structures to develop behind the front. These structures are able to grow in size owing to the favourable pressure gradient caused by the pycnocline deflection. In these experiments it appears that the internal wave crest speed is the same as the speed of these large billow structures, thus giving the appearance that the crest is 'locked' to these structures instead of the gravity current head. In figure 7(*c*) the interflow is seen entering the right of the frame, as it is moving much slower than the head of the gravity current.

#### 3.2.2. *Launched wave*

In the gravity current cases resulting in predominantly interflow, the initial intrusion appears to occur immediately below the pycnocline before returning upwards towards the static pycnocline level, possibly due to a competition between the initial downslope momentum and restoring force due to the positive buoyancy of the intrusion (Monaghan *et al.* 1999). The oscillatory movement of the gravity current then causes an internal wave to be initiated along the pycnocline well ahead of the intrusion as in figure 8(*a*), where a single wave crest can be observed slightly downstream of the intrusion. From figure 8(*b,c*), it is clear that the speed of the internal wave is faster than that of the intrusion or the head of the gravity current. The speed of this launched wave is thus not locked to the speed of the gravity current head. The wave speed is possibly set by the initial momentum and energy transferred from the gravity current, and may be restricted by ambient stratification conditions, including the height of the lower layer which increases until the end of the slope downstream.
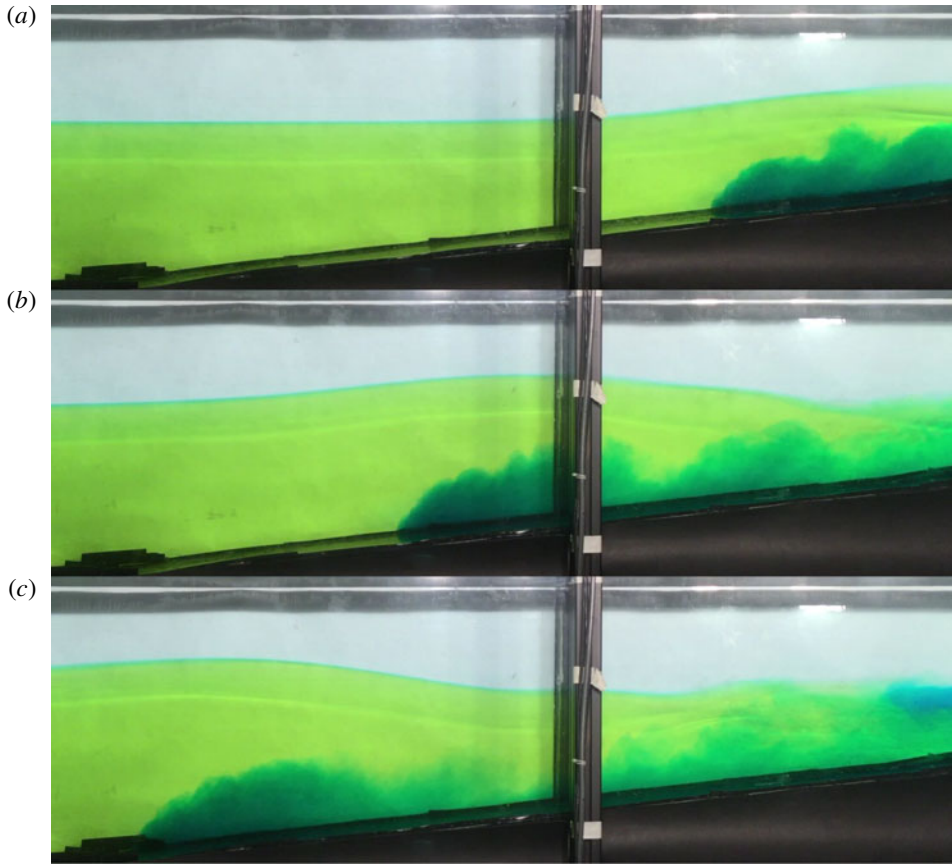
FIGURE 7. Progressive snapshots of a gravity current with $Ri_\rho = 1.7$ in the lower layer, where the crest of the pycnocline deflection is locked to the gravity current head.

### 3.2.3. *Comparing wave cases*

We formulate an internal wave Froude number $Fr$ (due to the gravity current) defined as

$$Fr = \frac{u_{GC}}{c_{IW}} \tag{3.4}$$

by tracking the frontal position of the gravity current and wave crest of the internal waves in each of the experiments, and fitting a linear function to find the velocities $u_{GC}$ and $c_{IW}$, respectively. For the locked case, we expect $Fr = 1$ since the progression of the gravity current head down the slope is the cause of the pycnocline deflection, suggesting that the two speeds should be equal. For the launched case, we expect $Fr < 1$ because the wave propagates along the pycnocline faster than any part of the gravity current, the majority of which has entered the ambient as an interflow. Generally, for the underflow-dominated locked-wave regime, only a small fraction of the gravity current tail will insert itself as an interflow; and for an interflow-dominated launched-wave case, only a small portion of the gravity current head will propagate as underflow. The concurrent occurrence of an underflow and interflow will cause both a locked and a launched wave (see, for example, figure 8*b,c*), although in most experiments we are only able to accurately measure the dominant wave.
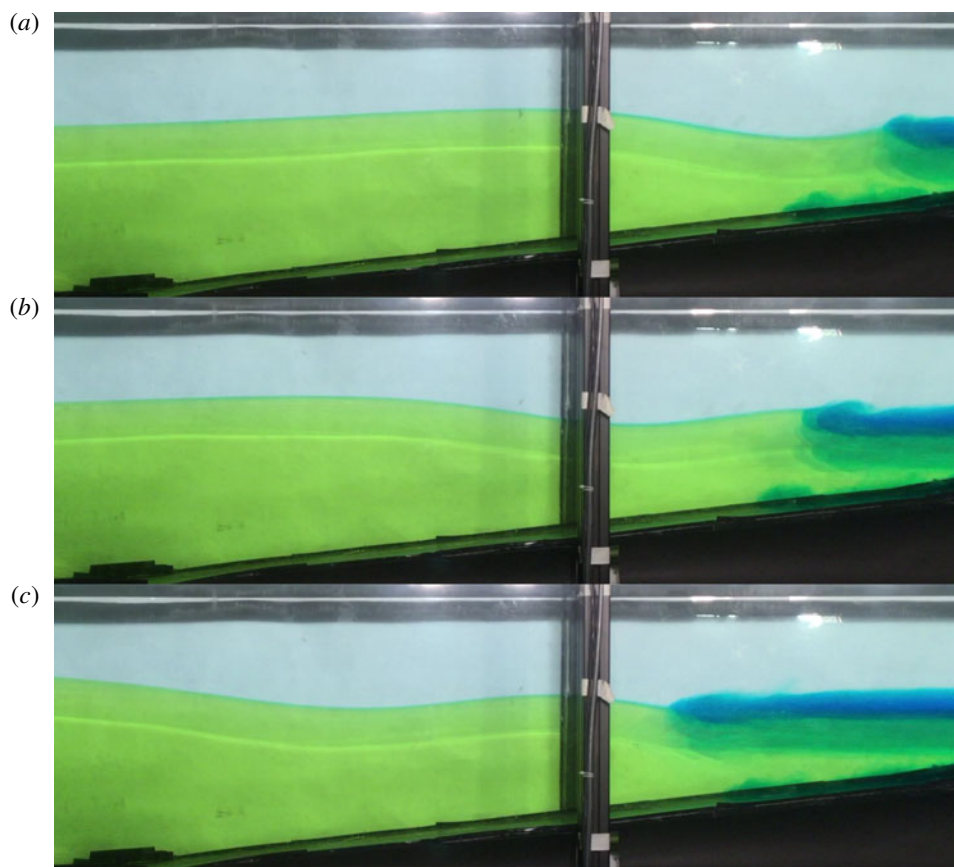
FIGURE 8. Progressive snapshots of a gravity current with $Ri_\rho = 3.7$. Here, the interfacial intrusion generates a wave that propagates downstream well ahead of the intrusion or the underflow gravity current head.

In some instances, there is enough underflow and interflow such that we observe a significant interaction between the two. In figure 9(a) the underflow is seen propagating in the lower layer, but the crest of the internal wave is downstream of the gravity current head, characteristic of a launched wave. As the interflow enters the frame in figure 9(b), the position of the crest of the wave has surpassed that of the gravity current head, and the trough of the wave appears to be interacting with the gravity current head and causing it to flatten out. The height of the underflow in figure 9(b) is much smaller compared to the typical gravity current head in figure 9(a) with many billows entraining the ambient fluid. In figure 9(c), the trough of the wave has passed the front of the underflow, and is now generating an adverse pressure gradient that slows down the underflow. An indication of this retarded underflow speed is seen by comparing figures 9(c) and 9(d). The interflow, which propagates from right to left, appears to be moving faster than the front of the underflow, which has propagated significantly less. Maxworthy *et al.* (2002) in experiments with horizontally propagating gravity currents in a linear stratification observed the same phenomenon, where the internal wave generated by the gravity current completely arrested the propagation of the head.
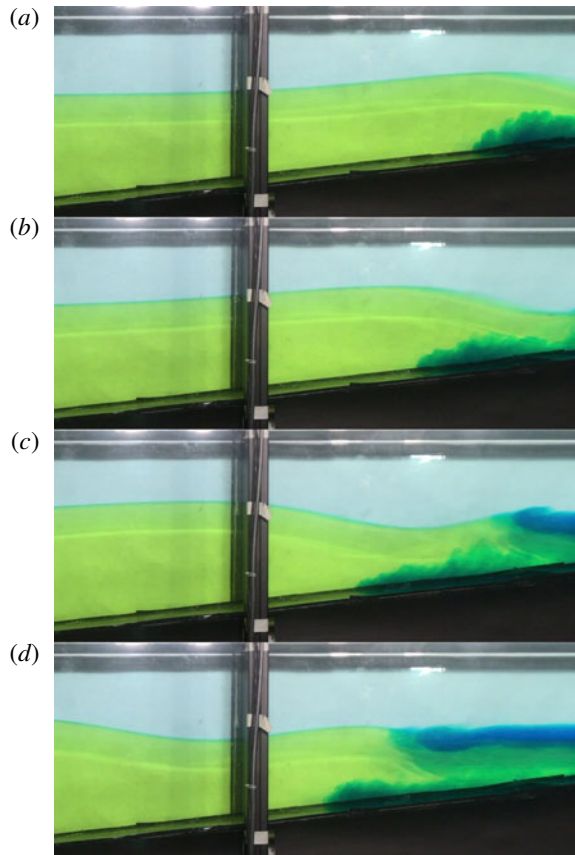
FIGURE 9. Progressive snapshots of a gravity current with $Ri_\rho = 3.1$. Here, the launched wave from the interfacial intrusion arrests the motion of the underflow.

Figure 10 shows the gravity current internal wave Froude number $Fr$ as a function of the gravity current Grashof number $Gr$. The uncertainty in the measurements arises from the imperfect tracking of the positions of the gravity current front and wave crest, and is a propagated 95 % confidence interval of the velocities. A low value of $Gr$ is suggestive of a weaker gravity current leading to an interflow-dominated situation, and a higher value of $Gr$ produces an underflow-dominated gravity current. For low $Gr$ cases, we find $Fr < 1$, consistent with the expected interflow-dominated regime. As $Gr$ is increased, $Fr$ also increases, and the majority of the cases for intermediate $Gr$ have $Fr$ between 0.9 and 1. For the larger $Gr$ cases, $Fr$ appears to be greater than 1, because the gravity current speed is measured to be greater than the internal wave speed. However, this brings into question to which part of the gravity current the wave is responding. This question arises because of the highly vortical nature of the head of the gravity current, where the locked wave speed may be dictated by the speed of the billow-like structure in the lee of the gravity current head as opposed to the frontal speed of the head itself. The behaviour of the leading billow structure is highly transient and it appears to grow in size due to a continuous generation of baroclinic vorticity as well as a potential interaction between the pycnocline deflection caused by the billow and the billow itself, thus allowing it
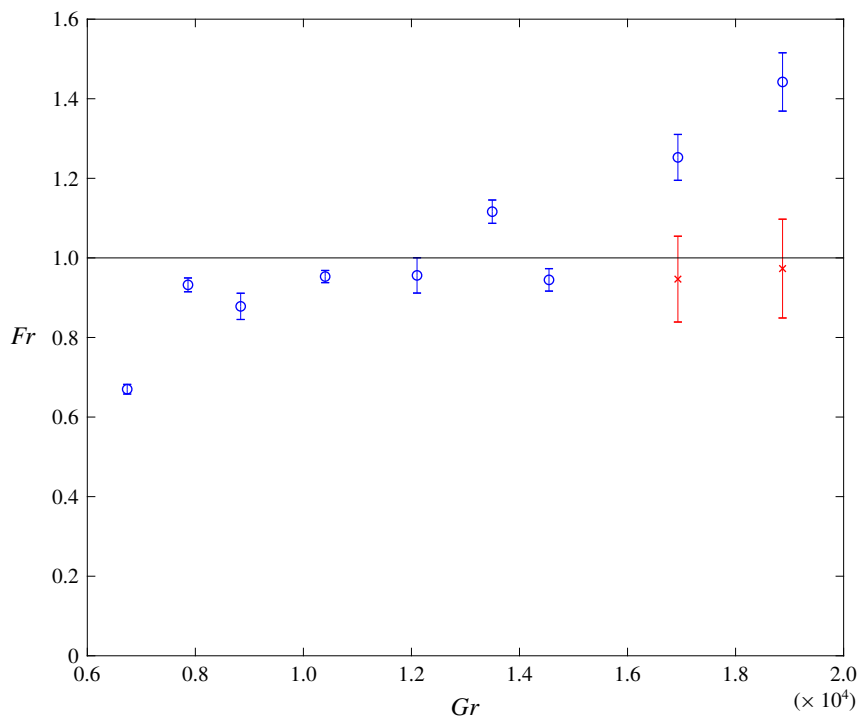
FIGURE 10. Froude number of the generated wave as a function of the Grashof number of
the gravity current. Circles show Froude numbers computed based on the gravity current
frontal speed, and crosses show Froude numbers computed based on the velocity of the
leading billow behind the head.

to grow. By measuring the propagation speed of the large billow structure behind the
head and recalculating $Fr$, the values become $Fr \approx 1$ as expected for the locked cases.
This result also suggests that there is a dispersive interaction between the head of the
gravity current and the large billow-like structure behind the head, causing the two
to separate from one another, a phenomenon that has not been observed in previous
studies of gravity currents propagating in homogeneous environments.

## 4. Discussion and conclusions

We used laboratory experiments to study the fate of negatively buoyant gravity
currents propagating down an inclined slope into a quiescent two-layer ambient
stratification. From vertical density profiles taken after the gravity current release, a
typical gravity current was identified as having formed both underflow and interflow.
Using hypothetical vertical density profiles as theoretical maximum and minimum
cases for underflow and interflow, the partitioning of the current into underflow and
interflow components was quantified using a non-dimensional centre of mass. By
using a Richardson number defined as the ratio between density excess of the gravity
current and the ambient stratification, a regime in which the splitting was a function
of $Ri_\rho$ was identified, along with asymptotic behaviour in the splitting for the gravity
currents tested.

Based on the final profiles as well as observations with tracer dye, gravity currents
with low Richardson numbers that predominantly result in underflow were observed

to also generate an interflow due to the transient interaction between the gravity current head and the pycnocline. The head of the gravity current vertically displaced the pycnocline, possibly creating an adverse pressure gradient for the tail portion of the gravity current and causing enhanced mixing to take place, leading to a following interflow. The consistent presence of an interflow is somewhat unexpected, and differs from the classical view of gravity currents in stratified media being either a pure underflow or interflow (Fischer *et al.* 1979).

Two different wave mechanisms were identified in the pycnocline response to the gravity current. In an underflow-dominated regime, the speed of the crest of the internal wave was locked to the speed of the head of the gravity current. For an interflow-dominated regime, the gravity current impinging on the pycnocline launched a wave that propagated faster than the gravity current head or interfacial intrusion. Using a Froude number comparing the speed of the gravity current to the phase speed of the wave, we characterized the launched and locked regimes. In gravity currents with the highest buoyancy flux and therefore Grashof number, we found that the internal wave was not in fact locked to the speed of the front of the gravity current but rather to the speed of the leading billow-like structure behind the head of the current.

A potential limitation to the generalization of the results presented regarding the quantification of the splitting of the gravity current is related to the shape of the vertical density and velocity profiles of the gravity current. Cortés *et al.* (2014*b*) measured both the density and velocity profiles of the gravity current and compared them to previous studies. Although trends were generally consistent for both subcritical and supercritical gravity currents, there were differences in the shapes of the gravity current profiles, and Cortés *et al.* (2014*b*) showed that this would have an impact on the splitting behaviour of the gravity current. Currently there is no unifying theory or dimensionless parameter to describe the structure of the density and velocity profiles of a gravity current, which would ultimately lead to a more generalized parameterization of its splitting. While the splitting transitional $Ri_\rho$ and resulting $M_c^*$ may vary due to varying shapes of the velocity and density profiles, there are two more generalizable results emerging from our work that should apply to stratified water bodies in general. First, we can expect that a dense gravity current in a stratified system will undergo some degree of splitting, and exhibit both underflow and interflow characteristics compared to the more traditional thinking of gravity currents being purely underflow or purely interflow. Second, upon reaching the pycnocline, the underflow portion of the gravity current will produce a locked wave at the interface, while the interflow part will produce a launched wave at the interface.

## Acknowledgements

## Declaration of interests

The authors report no conflict of interest.

# REFERENCES

ACHESON, D. J. 1990 *Elementary Fluid Dynamics*. Clarendon Press; Oxford University Press.

ARTHUR, R. S. & FRINGER, O. B. 2014 The dynamics of breaking internal solitary waves on slopes. *J. Fluid Mech.* **761**, 360–398.

BAINES, P. G. 2001 Mixing in flows down gentle slopes into stratified environments. *J. Fluid Mech.* **443**, 237–270.

BAINES, P. G. 2008 Mixing in downslope flows in the ocean – plumes versus gravity currents. *Atmos.-Ocean* **46** (4), 405–419.

BENJAMIN, T. B. 1968 Gravity currents and related phenomena. *J. Fluid Mech.* **31** (2), 209–248.

BRITTER, R. E. & LINDEN, P. F. 1980 The motion of the front of a gravity current travelling down an incline. *J. Fluid Mech.* **99** (03), 531–543.

BRITTER, R. E. & SIMPSON, J. E. 1978 Experiments on the dynamics of a gravity current head. *J. Fluid Mech.* **88** (2), 223–240.

BRITTER, R. E. & SIMPSON, J. E. 1981 A note on the structure of the head of an intrusive gravity current. *J. Fluid Mech.* **112**, 459–466.

CENEDESE, C. & ADDUCE, C. 2010 A new parameterization for entrainment in overflows. *J. Phys. Oceanogr.* **40** (8), 1835–1850.

CHAPRA, S. C. 1997 *Surface Water-Quality Modeling*. WCB/McGraw-Hill.

CHEONG, H. B., KUENEN, J. J. P. & LINDEN, P. F. 2006 The front speed of intrusive gravity currents. *J. Fluid Mech.* **552**, 1–11.

CORTÉS, A., FLEENOR, W. E., WELLS, M. G., DE VICENTE, I. & RUEDA, F. J. 2014a Pathways of river water to the surface layers of stratified reservoirs. *Limnol. Oceanogr.* **59** (1), 233–250.

CORTÉS, A., RUEDA, F. J. & WELLS, M. G. 2014b Experimental observations of the splitting of a gravity current at a density step in a stratified water body. *J. Geophys. Res. Oceans* **119** (2), 1038–1053.

CORTÉS, A., WELLS, M. G., FRINGER, O. B., ARTHUR, R. S. & RUEDA, F. J. 2015 Numerical investigation of split flows by gravity currents into two-layered stratified water bodies. *J. Geophys. Res. C: Oceans* **120** (7), 5254–5271.

CRIMALDI, J. P. & KOSEFF, J. R. 2001 High-resolution measurements of the spatial and temporal scalar structure of a turbulent plume. *Exp. Fluids* **31** (1), 90–102.

DALLIMORE, C. J., IMBERGER, J. & ISHIKAWA, T. 2002 Entrainment and turbulence in saline underflow in lake Ogawara. *ASCE J. Hydraul. Engng* **127** (11), 937–948.

DAVIS, K. A. & MONISMITH, S. G. 2011 The modification of bottom boundary layer turbulence and mixing by internal waves shoaling on a barrier reef. *J. Phys. Oceanogr.* **41** (11), 2223–2241.

ELLISON, T. H. & TURNER, J. S. 1959 Turbulent entrainment in stratified flows. *J. Fluid Mech.* **6** (03), 423–448.

FERNANDEZ, R. L. & IMBERGER, J. 2006 Bed roughness induced entrainment in a high Richardson number underflow. *J. Hydraul Res.* **44** (6), 725–738.

FERNÁNDEZ-TORQUEMADA, Y., GÓNZALEZ-CORREA, J. M., LOYA, A., FERRERO, L. M., DÍAZ-VALDÉS, M. & SÁNCHEZ-LIZASO, J. L. 2009 Dispersion of brine discharge from seawater reverse osmosis desalination plants. *Desalin. Water Treat.* **5** (1–3), 137–145.

FISCHER, H. B., KOH, R., LIST, J. E., KOH, C. R., IMBERGER, J. & BROOKS, N. H. 1979 *Mixing in Inland and Coastal Waters*. Academic Press.

FISCHER, H. B. & SMITH, R. D. 1983 Observations of transport to surface waters from a plunging inflow to lake Mead. *Limnol. Oceanogr.* **28** (2), 258–272.

FLYNN, M. R. & LINDEN, P. F. 2006 Intrusive gravity currents. *J. Fluid Mech.* **568**, 193–202.

FLYNN, M. R. & SUTHERLAND, B. R. 2004 Intrusive gravity currents and internal gravity wave generation in stratified fluid. *J. Fluid Mech.* **514**, 355–383.

FRINGER, O. B. & STREET, R. L. 2003 The dynamics of breaking progressive interfacial waves. *J. Fluid Mech.* **494**, 319–353.

HALLWORTH, M. A., HOGG, A. J. & HUPPERT, H. E. 1998 Effects of external flow on compositional and particle gravity currents. *J. Fluid Mech.* **359**, 109–142.

HALLWORTH, M. A., HUPPERT, H. E., PHILLIPS, J. C. & SPARKS, R. S. J. 1996 Entrainment into two-dimensional and axisymmetric turbulent gravity currents. *J. Fluid Mech.* **308**, 289–311.

HEBBERT, B., PATTERSON, J., LOH, I. & IMBERGER, J. 1979 Collie river underflow into the Wellington reservoir. *J. Hydraul. Div.* **105** (5), 533–545.

HODGES, B. R., FURNANS, J. E. & KULIS, P. S. 2011 Thin-layer gravity current with implications for desalination brine disposal. *ASCE J. Hydraul. Engng* **137** (3), 356–371.

HOGG, C. A. R., EGAN, G., OUELLETTE, N. T. & KOSEFF, J. R. 2017 Shoaling internal waves may reduce gravity current transport. *Environ. Fluid Mech.* **18** (2), 383–394.

HOGG, C. A. R., MARTI, C. L., HUPPERT, H. E. & IMBERGER, J. 2013 Mixing of an interflow into the ambient water of lake Iseo. *Limnol. Oceanogr.* **58** (2), 579–592.

HOGG, C. A. R., PIETRASZ, V., EGAN, G., OUELLETTE, N. T. & KOSEFF, J. R. 2016 The influence of a shoaling internal gravity wave on a dense gravity current. In *VIIIth International Symposium on Stratified Flows, San Diego, CA, USA*, vol. 1 (1).

HOLYER, J. Y. & HUPPERT, H. E. 1980 Gravity currents entering a two-layer fluid. *J. Fluid Mech.* **100** (4), 739–767.

HULT, E. L., TROY, C. D. & KOSEFF, J. R. 2011 The mixing efficiency of interfacial waves breaking at a ridge: 1. Overall mixing efficiency. *J. Geophys. Res. Oceans* **116** (2), 1–10.

HUPPERT, H. E. & DADE, W. B. 1998 Natural disasters: explosive volcanic eruptions and gigantic landslides. *Theor. Comput. Fluid Dyn.* **10** (1), 201–212.

JENKINS, S., PADUAN, J., ROBERTS, P., SCHLENK, D. & WEIS, J. 2012 Management of brine discharges to coastal waters recommendations of a science advisory panel. In *Southern California Coastal Water Research Project. Costa Mesa, CA*.

KRUG, D., HOLZNER, M., LÜTHI, B., WOLF, M., KINZELBACH, W. & TSINOBER, A. 2015 The turbulent/non-turbulent interface in an inclined dense gravity current. *J. Fluid Mech.* **765**, 303–324.

KVITEK, R. G., CONLAN, K. E. & IAMPIETRO, P. J. 1998 Black pools of death: Hypoxic, brine-filled ice gouge depressions become lethal traps for benthic organisms in a shallow Arctic embayment. *Mar. Ecol. Progress Series* **162**, 1–10.

LATTEMANN, S. & AMY, G. 2013 Marine monitoring surveys for desalination plants – a critical review. *Desalin. Water Treat.* **51** (1–3), 233–245.

LINDEN, P. F. & SIMPSON, J. E. 1986 Gravity-driven flows in a turbulent fluid. *J. Fluid Mech.* **172**, 481–497.

LONG, R. R. 1956 Solitary waves in the one- and two-fluid systems. *Tellus* **8** (4), 460–471.

LOWE, R. J., LINDEN, P. F. & ROTTMAN, J. W. 2002 A laboratory study of the velocity structure in an intrusive gravity current. *J. Fluid Mech.* **456**, 33–48.

MACINTYRE, S., FLYNN, K. M., JELLISON, R. & ROMERO, J. 1999 Boundary mixing and nutrient fluxes in Mono Lake, California. *Limnol. Oceanogr.* **44** (3), 512–529.

MARTI, C. L. & IMBERGER, J. 2008 Exchange between littoral and pelagic waters in a stratified lake due to wind-induced motions: Lake Kinneret, Israel. *Hydrobiologia* **603** (1), 25–51.

MASUNAGA, E., FRINGER, O. B. & YAMAZAKI, H. 2016 An observational and numerical study of river plume dynamics in Otsuchi Bay, Japan. *J. Oceanogr.* **72** (1), 3–21.

MAURER, B. D. & LINDEN, P. F. 2014 Intrusion-generated waves in a linearly stratified fluid. *J. Fluid Mech.* **752**, 282–295.

MAXWORTHY, T., LEILICH, J., SIMPSON, J. E. & MEIBURG, E. H. 2002 The propagation of a gravity current into a linearly stratified fluid. *J. Fluid Mech.* **453**, 371–394.

MEIBURG, E. H. & KNELLER, B. 2010 Turbidity currents and their deposits. *Annu. Rev. Fluid Mech.* **42** (1), 135–156.

MISSIMER, T. M. & MALIVA, R. G. 2017 Environmental issues in seawater reverse osmosis desalination: Intakes and outfalls. *Desalination* **434** (April 2017), 198–215.

MONAGHAN, J. J. 2007 Gravity current interaction with interfaces. *Annu. Rev. Fluid Mech.* **39**, 245–261.

MONAGHAN, J. J., CAS, R. A. F., KOS, A. M. & HALLWORTH, M. 1999 Gravity currents descending a ramp in a stratified tank. *J. Fluid Mech.* **379**, 39–69.

MOORE, C. D., KOSEFF, J. R. & HULT, E. L. 2016 Characteristics of bolus formation and propagation from breaking internal waves on shelf slopes. *J. Fluid Mech.* **791**, 260–283.

MOTT, R. W. & WOODS, A. W. 2009 On the mixing of a confined stratified fluid by a turbulent buoyant plume. *J. Fluid Mech.* **623**, 149–165.

MULDER, T. & ALEXANDER, J. 2001 The physical character of subaqueous sedimentary density flows and their deposits. *Sedimentology* **48** (2), 269–299.

NEGRETTI, M. E., FLÒR, J. B. & HOPFINGER, E. J. 2017 Development of gravity currents on rapidly changing slopes. *J. Fluid Mech.* **833**, 70–97.

ODIER, P., CHEN, J. & ECKE, R. E. 2012 Understanding and modeling turbulent fluxes and entrainment in a gravity current. *Physica* D *Nonlinear Phenomena* **241** (3), 260–268.

ODIER, P., CHEN, J. & ECKE, R. E. 2014 Entrainment and mixing in a laboratory model of oceanic overflow. *J. Fluid Mech.* **746** (3), 498–535.

REHMANN, C. R. 1995. Effects of stratification and molecular diffusivity on the mixing efficiency of decaying grid turbulence. PhD thesis, Stanford University.

ROBERTS, D. A., JOHNSTON, E. L. & KNOTT, N. A. 2010 Impacts of desalination plant discharges on the marine environment: a critical review of published studies. *Water Res.* **44** (18), 5117–5128.

ROBINSON, T. O., EAMES, I. & SIMONS, R. 2013 Dense gravity currents moving beneath progressive free-surface water waves. *J. Fluid Mech.* **725**, 588–610.

RUEDA, F. J., FLEENOR, W. E. & DE VICENTE, I. 2007 Pathways of river nutrients towards the euphotic zone in a deep-reservoir of small size: uncertainty analysis. *Ecol. Model.* **202** (3), 345–361.

SAMOTHRAKIS, P. & COTEL, A. J. 2006a Finite volume gravity currents impinging on a stratified interface. *Exp. Fluids* **41** (6), 991–1003.

SAMOTHRAKIS, P. & COTEL, A. J. 2006b Propagation of a gravity current in a two-layer stratified environment. *J. Geophys. Res. Oceans* **111**, C01012.

SHIN, J. 2001 Colliding gravity currents. PhD thesis, Cambridge University.

SIMPSON, J. E. 1982 Gravity currents in the laboratory, atmosphere, and ocean. *Annu. Rev. Fluid Mech.* **14** (1), 213–234.

SIMPSON, J. E. 1997 *Gravity Currents: in the Environment and the Laboratory*. Cambridge University Press.

SIMPSON, J. E. & BRITTER, R. E. 1979 The dynamics of the head of a gravity current advancing over a horizontal surface. *J. Fluid Mech.* **94** (3), 477–495.

SOVILLA, B., MCELWAINE, J. N. & KÖHLER, A. 2018 The intermittency regions of powder snow avalanches. *J. Geophys. Res. Earth Surf.* **123** (10), 2525–2545.

SUTHERLAND, B. R., KYBA, P. J. & FLYNN, M. R. 2004 Intrusive gravity currents in two-layer fluids. *J. Fluid Mech.* **514**, 327–353.

TROY, C. D. & KOSEFF, J. R. 2005a The generation and quantitative visualization of breaking internal waves. *Exp. Fluids* **38** (5), 549–562.

TROY, C. D. & KOSEFF, J. R. 2005b The instability and breaking of long internal waves. *J. Fluid Mech.* **543**, 107–136.

TURNER, J. S. 1986 Turbulent entrainment: the development of the entrainment assumption, and its application to geophysical flows. *J. Fluid Mech.* **173**, 431–471.

UNGARISH, M. & HUPPERT, H. E. 2002 On gravity currents propagating at the base of a stratified fluid. *J. Fluid Mech.* **458**, 283–301.

VENAYAGAMOORTHY, S. K. & FRINGER, O. B. 2007 On the formation and propagation of nonlinear internal boluses across a shelf break. *J. Fluid Mech.* **577**, 137–159.

WALLACE, R. B. & SHEFF, B. B. 1987 Two-dimensional buoyant jets in two-layer ambient fluid. *ASCE J. Hydraul. Engng* **113** (8), 992–1005.

WALTER, R. K., WOODSON, B. C., ARTHUR, R. S., FRINGER, O. B. & MONISMITH, S. G. 2012 Nearshore internal bores and turbulent mixing in southern Monterey Bay. *J. Geophys. Res. Oceans* **117** (7), 1–13.

WELLS, M. G. & WETTLAUFER, J. S. 2007 The long-term circulation driven by density currents in a two-layer stratified basin. *J. Fluid Mech.* **572**, 37–58.